Journal of Hydrology 565 (2018) 636–649

Contents lists available at ScienceDirect

Journal of Hydrology

journal homepage: www.elsevier.com/locate/jhydrol

Research papers

Impact of historic and future climate on spring recharge and discharge based on an integrated numerical modelling approach: Application on a snow-governed semi-arid karst catchment area

Joanna Doummar[a,*], Assaad Hassan Kassem[a], Jason J. Gurdak[b]

[a] Department of Geology, American University of Beirut, PO Box: 11-0236/26, Beirut, Lebanon
[b] San Francisco State University, Department of Earth & Climate Sciences, 1600 Holloway Avenue, San Francisco, CA 94132, USA

ARTICLE INFO

This manuscript was handled by Marco Borga, Editor-in-Chief, with the assistance of Massimiliano Zappa, Associate Editor

Keywords:
Karst
Climate change
Integrated numerical modelling

ABSTRACT

Flow in a karst system in Lebanon (Important water supply source; Assal Spring; discharge 0.2–2.5 m^3/s yearly volume of 22–30 Mm^3), which is dominated by snow and semi-arid conditions, was simulated using an integrated numerical model (Mike She, 2016). The calibrated model (Nash–Sutcliffe coefficient of 0.77) is based on high resolution input data (2014–2017) and detailed catchment characterization. A sensitivity analysis of individual climatic parameters shows that spring hydrograph characteristics are most sensitive to temperature.

A forward simulation using the IPS_cm5 model with the RCP6.0 scenario for future climate change (Global Climate Models GCM; daily downscaled bias and altitude corrected time series for Lebanon 2020–2099) unravel that precipitation, recharge, and discharge have moderate to highly significant decreasing trends with time over the 21st century. Moreover, recession flowrates are expected to drop drastically starting in the year 2070 to 1 l/s with shortage periods reaching up to six months. The latter is due to a temperature rise of +1.5–2.5 °C and subsequent shrinking of snow cover by almost 100% (e.g., 2073–2074). Furthermore, this is accompanied by a decline in annual spring volume by 73% with respect to the current status, with real evapotranspiration consisting of up to 50% from total water budget (currently around 12–17% in 2014–2017). Moreover, decreasing snow accumulation and a more prominent flushing of precipitation event waters into fast preferential pathways will lead to peak spring discharges. This study allows decision makers to implement best informed practices for future water resources management especially for karst systems under semi-arid conditions in the regions.

1. Introduction

Freshwater has been under stress in recent decades due to climate change and increasing water demands (Kløve et al., 2014). In response, numerous water management methods have been developed (Iglesias et al., 2007) to overcome water shortage, prevent further degradation of groundwater quality and quantity, and ensure sustainable water supply in the future (Taylor et al., 2013). Several studies aimed at highlighting the impact of climate change on groundwater resources (Gleeson et al., 2012; Green et al., 2011; Goderniaux et al., 2015) to assess the extent of the problem and to ensure that management and sustainable exploitation practices account for future climatic variability and increasing demand (Hartmann et al., 2012; Lauffenburger et al., 2018; Loaiciga et al., 2000; Neves et al, 2016; Samuels et al., 2010).

Fresh water availability and recharge is affected by climatic parameters; namely precipitation, temperature, and evaporation (Bates et al., 2008) in addition to land use and land cover, as well as the response of specific types of aquifer. The development and application of integrated groundwater flow and solute transport models are ideal tools for decision makers to predict the transient behavior of aquifers under various stress conditions such as decrease of precipitation, increase of temperature (Christensen et al., 2007; Hartmann et al., 2014) and increased likelihood of floods or droughts (Hartmann et al., 2017; Taylor et al., 2013).

Several previous studies have simulated groundwater responses (water availability, total recharge, water table fluctuations) to various future climatic scenarios in different climate regions (Bliss et al., 2014; Hartmann et al., 2014; Khadka et al., 2014; Stigter et al., 2014; Yang et al., 2014; Mountain Research Initiative EDW Working Group, 2015; Beniston and Stoffel, 2016; Kopsiaftis et al., 2017). For example, the Mediterranean region is expected to undergo pronounced droughts periods and a subsequent unusual decline of groundwater resources

* Corresponding author.
E-mail address: jd31@aub.edu.lb (J. Doummar).

https://doi.org/10.1016/j.jhydrol.2018.08.062
Received 7 March 2018; Received in revised form 15 August 2018; Accepted 27 August 2018
Available online 29 August 2018

(Giorgi and Lionello, 2008). Additionally, other studies have taken into account the effect of the anthropogenic activities such as over-pumping and increase in population and water demand on future groundwater resources (Dar et al., 2014; Gurdak, 2017; Sapriza-Azuri et al., 2015; Sharma et al., 2015; Hartmann et al., 2016; Shrestha et al., 2016). In another example from a catchment in the Mediterranean region, hydrological model simulations to future climate change and increase in pumping predicted a 3-month extended dry period in the future, in addition to a 50% decline in groundwater recharge and a 20% increase in evapotranspiration (Sapriza-Azuri et al., 2015). Other parameters such as groundwater- surface water exchange, stream flow, and runoff generation were also expected to decrease by 60% (Sapriza-Azuri et al., 2015). While the future variation in precipitation patterns negligibly affects stream responses to precipitation, a considerable increase in evaporation and decrease in rainfall amount is to be expected in the future (Samuels et al., 2010). Sharma et al. (2015), shows that the estimated change in temperature (an increase of 0.32–1.28 °C) in years 2021–2051 will result in an annual decline in groundwater level by 4.6% and 17.8% in 2021 and 2051, respectively. It was also noted that climate variation might become more pronounced in the future, which may have escalating effects on groundwater sustainability (Sharma et al., 2015). Moreover, rainfall under tropical conditions is thought to decrease in the dry season and to increase in the wet season (Shrestha et al., 2016). An application using projections based on future Representative Concentrating Pathways (RCPs) scenarios (Van Vuuren, et al., 2011), shows that the expected change in temperature by the end of the 21st century ranging between +1.5 °C and +4.9 °C, will yield an important decrease in groundwater recharge and therefore water level and storage (Shrestha et al., 2016).

In such groundwater and climate change simulations, the validity of the predicted output depends to a large extent on the resolution, uncertainty, and uniqueness of the base hydrological model. Unlike most porous unconsolidated systems, the selection and construction of a hydrological model for future projections is particularly challenging in highly responsive karst aquifers systems due to their duality of infiltration and flow (Kiraly, 2002; Geyer et al., 2008). The duality of flow requires the simulation of both fast (high response to precipitation events) and slow flow components (Birk et al., 2004; Geyer et al., 2008). Moreover, as karst aquifers have been known to be highly impacted by environmental changes (Butscher and Huggenberger, 2009; Ravbar et al., 2017), their sensitivity to climate change has been recently given particular attention (Hartmann et al., 2014; Charlier et al., 2015; Chen et al., 2017; Hao et al., 2006; Loaiciga et al., 2000; Samuels et al., 2010). Hartmann et al. (2014) used a combination of spatially distributed recharge as percentage of precipitation (Andreo et al., 2008) and a process based lumped model and others such as Hao et al. (2000) applied a gray-box model to simulate variation of recharge rate, discharge and their relationship to precipitation under future climatic variability in a Mediterranean karst region (Hartmann et al., 2012; Samuels et al., 2010). It is worth noting that simulation of this type of aquifer requires both high resolution time series and detailed catchment characterization (Ranjan et al., 2006) to account for the spatial distribution of point source fast infiltration, land use, and soil type distribution, which are key parameters in climatic components such as evapotranspiration (Manrique-Alba et al., 2017). Such information may be scarce and unavailable at the scale of a catchment, but is needed to set up and calibrate a representative integrated hydrogeological model valid for future climate scenarios simulations (Taylor et al., 2013).

The aim of this study is to use a spatially distributed model to simulate the response of an important karst spring in Lebanon to future climatic scenarios based on bias corrected downscaled projected climatic data for the region. Flow in the small-scale pilot catchment (influenced highly by snowmelt in a semi-arid region) was simulated with an integrated process based hydrological model MIKE She (DHI, 2016) to account for the atmosphere, unsaturated zone, and saturated zone, and depict the variation of response signals in each of these layers. Snow melt was regarded as an important factor controlling recharge processes in snow dominated areas (Chen et al. 2017). The calibrated and validated model is based on high resolution collected data for spring discharge and climatic parameters (2014–2017) and detailed catchment characterization from tracer experiments and soil sampling. The influence of climate change is evaluated using two approaches. First, we evaluated the sensitivity of spring discharge to historical climate data, such as precipitation (P) and temperature (T), etc. Second, we conducted future flow simulations using downscaled data from the IPSL_CM5 global climate model (GCM) with Representative Concentration Pathway (RCP) 6.0 scenario to depict the daily variation of discharge in 2021–2099. The study further highlights the variation of recession coefficients with time that is indicative of the flow pathways, duration of the recession periods below a specific threshold, and the lag of spring response to snowmelt under future climatic conditions. These findings have important implications for water management decisions and policy in similar catchment types across the greater Mediterranean region.

2. Methodology

In the framework of a monitoring project funded by USAID since 2014, a full climatic station (Campbell-Scientific-Alpine type) with a heated gauge mounted with a data logger was installed at about 1700 m above sea level to record climatic parameters such as precipitation, temperature, humidity, wind direction and speed, and radiation at an hour interval. Additionally, a multi parameter probe (Insitu-Troll 9500) measuring parameters such as water level, electrical conductivity, temperature, turbidity, chloride, pH and Redox potential at a 30-min interval. Daily data for these parameters was obtained/ purchased from local authorities for the period extending from 2010 till 2013. A rating curve (polynomial relationship) between water level and discharge was constructed based on bi-monthly measured discharge rate over a period of two years. The error of the measurement is about 8–10% during recession. The methods to develop a calibrated integrated hydrological model to simulate spring responses to future climatic scenarios use the following three consecutive steps (Fig. 1):

(1) Construct an integrated numerical model with MIKE She (DHI, 2016) with high resolution time series data (2010–2015) based on detailed geological characterization, calibrate the model based on spring discharge data, and to validate it (2015–2017);
(2) Perform sensitivity analysis on single climate parameters such as precipitation and temperature to evaluate their impact on the modelling results; and
(3) Conduct future simulations (2020–2099) based on time series of forecast climatic data downscaled from a GCM, apply different statistical tests for distribution and significance, and highlight the impact of climate change scenarios on spring discharge and on different signals within the various hydrologic compartments in the karst system and other spring characteristics.

2.1. Set up and calibration of an integrated hydrological model

In this work, the simulation of flow in a karst system at a catchment scale was done using MIKE She (DHI, 2016). The catchment area of a karst spring is sub-divided spatially into a 33 × 33-m cell size grid and vertically into three main compartments: atmosphere (A), unsaturated zone (UZ), and saturated zone (SZ). The development of the model and its parametrization was based on a similar approach used in Doummar et al. (2012) with the same set of calibration parameters (fitted and physically based parameters).

The A compartment includes climatic processes (rainfall, snow, evapotranspiration) and interception by vegetation. The snow model used for the purpose of this study is a simple one governed mostly by air temperature (DHI, 2016). If air temperature is above the threshold

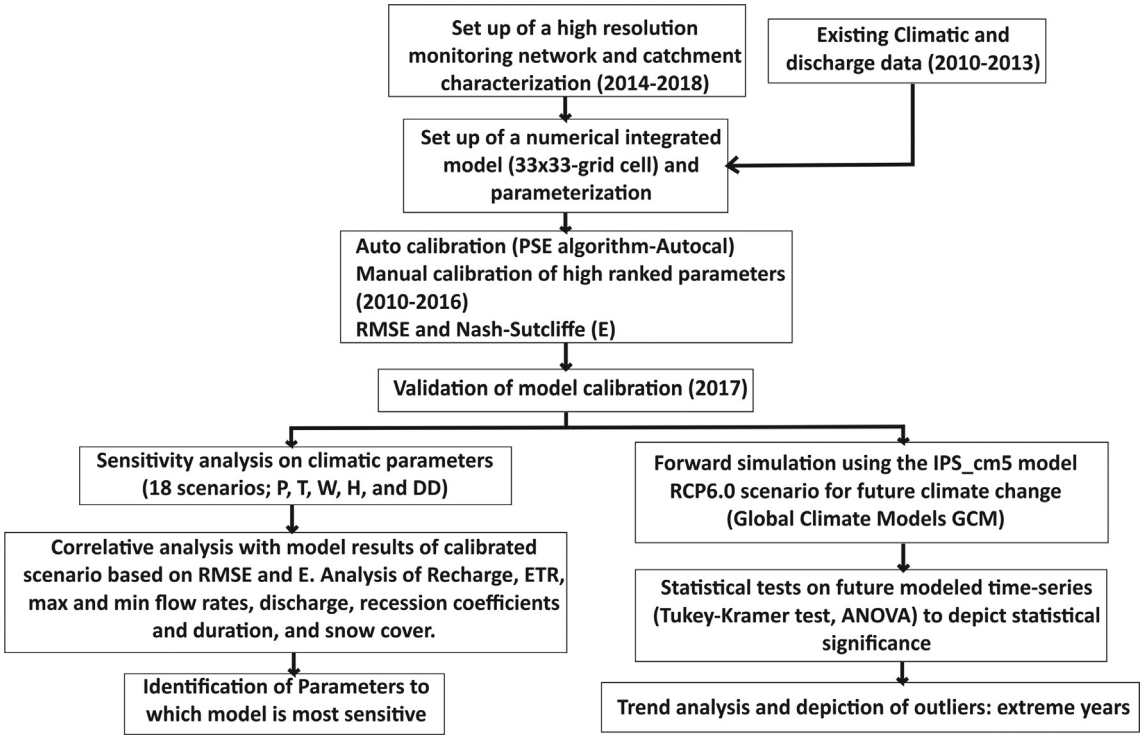

Fig. 1. Flow chart illustrating the various steps adopted in this work from monitoring to the integrated numerical modelling (calibration, validation, and sensitivity analysis) prior to model simulation under future climatic conditions.

melting temperature, then the snow will begin to melt according to:

$$M_T = \mathrm{DD}(T_{air} - \mathrm{T_0}) \quad (1)$$

where M_T is the rate of melting due to the air temperature, DD is the degree day factor for snow melting that reflects the amount of snow melt per positive degree day mm/°C/day; (Zuzel and Cox, 1975), T_{air} is the air temperature of the cell spatially variant, and $\mathrm{T_0}$ is the threshold melting temperature considered as invariant. The air temperature melting will be positive if the air temperature is above the threshold temperature and negative if it is below. Thus, if the air temperature falls below the threshold melting temperature, then wet snow will be re-converted back to dry snow.

The UZ represents the unsaturated zone below land surface governed by drainage by gravity in 1-D. Parameterization of the UZ includes calibrated physical properties of the soils and epikarst. The epikarst layer simulates the properties of the unsaturated rock matrix. The bypass function in MIKE She allows for the simulation of the fast flow component (rapid recharge), by routing infiltrating water directly to the groundwater table.

The bypass flow is calculated as a fraction of the net rainfall for each UZ time step. The actual bypass fraction is a function of a user-specified maximum fraction and the actual water content of the unsaturated zone, assuming macropore flow only in wet conditions (DHI, 2016). Thus, the bypass flow is distributed spatially differently in diffuse (bare rocks) and point source infiltration points (dolines) and is calculated as follows:

$$Q_{bypass} = P_{net} P_{frac} \sqrt{\alpha_{10}\beta_{50}} / \Delta T \quad (2)$$

where $\mathrm{P_{net}}$ is the net rainfall rate, and $\mathrm{P_{frac}}$ is the maximum fraction of the net rainfall which can bypass the matrix (under wet conditions). α_{10} and β_{50} are used to reduce the total bypass fraction under dry conditions calculated depending on user- input values and the actual water contents of the unsaturated zone 10 cm and 50 cm below the ground surface, respectively.

The SZ is simulated as a continuum using 3-D finite differences, with an incorporated zone of high hydraulic conductivity representing pathways of high groundwater velocities (e.g., ephemeral valleys believed to be preferential pathways; Taylor et al., 2013; Xanke et al., 2016).

The calibration was performed using the AutoCal by Mike She (based on a Population Simplex Evolution PSE optimization algorithm) for the years 2010 and 2016, and refined on the high resolution monitored years (2014–2016), while validation was done for year 2017. Additionally, calibration was done manually to refine selected parameters based on their impact on model results as per Doummar et al. (2012). The model output data were compared with daily observed discharge (downscaled from 30-min monitoring at the spring since 2014), using objective functions such as residual mean square error (RMSE) and the Nash Sutcliffe efficiency (E) coefficient. The RMSE and E are defined as follows:

$$RMSE = \sqrt{\frac{1}{n}\sum_{i=1}^{n}(c_i - c)^2} \quad (3)$$

$$E = 1 - \frac{\sum (c_i - c)^2}{\sum \left(c_i - \frac{1}{n}(\sum c_i)\right)^2} \quad (4)$$

where c_i is the simulated value at t_i and c is the calibrated value.

2.2. Sensitivity analysis on single climatic parameters

The spring discharge sensitivity to precipitation, temperature, temperature and precipitation lapse rates (variation of precipitation amount and temperature with 100 m elevation), wind and humidity, and degree day coefficient was investigated using 17 different scenarios (Table 1). The results of these scenarios are compared to the baseline scenario for the hydrogeological year 2016–2017. The selection of the different scenarios relied on historical climate variability from the study area and existing literature. The −20 to +20% variation in precipitation was based on the variation of percent change in simulated average annual precipitation observed from 16 global climatic models (GCMs) under high global warming conditions (Lauffenburger et al., 2018). The

Table 1
Scenarios assessing the sensitivity of single climate parameters on the model results.

	Scenario	Description	Parameter change
0	Calibrated	Baseline model 2016–2017	–
1	P20	Baseline daily precipitation increased by 20%	Precipitation (+20%)
2	P-20	Baseline daily precipitation decreased by 20%	Precipitation (−20%)
3	Plapse1	Precipitation lapse per altitude of 1% per 100 m (calibrated 6% per 100 m)	Precipitation (−15%)
4	Plapse3	Precipitation lapse per altitude of 3% per 100 m	Precipitation (−9%)
5	Plapse8	Precipitation lapse per altitude of 8% per 100 m	Precipitation (+6%)
6	T20	An increase of 20% in the daily observed entry temperature (2015–2017)	Temperature (+20%)
7	T−20	A decrease of 20% in the daily observed entry temperature (2015–2017)	Temperature (−20%)
8	T+2 °C	An increase of the temperature of +2 °C (max entry temperature of 30 °C)	Average temperature; +35% of T_{min}
9	T−2 °C	A decrease of the temperature of −2°C (max entry temperature of 25.5 °C)	Average temperature; −35% of T_{min}
10	Tlapse-0.75	Temperature lapse per altitude of −0.75 °C per 100 m (calibrated −0.45 °C per 100 m)	Temperature (−3%)
11	Tlapse-0.15	Temperature lapse per altitude of −0.15 °C per 100 m (calibrated −0.45 °C per 100 m)	Temperature (+3%)
12	W-20	A decrease of 20% in the daily observed wind speed (2015–2017), effect on ET reference	Wind (−20%)
13	W20	An increase of 20% in the daily observed wind speed (2015–2017), effect on ET reference	Wind (+20%)
14	H20	An increase of 20% in the daily observed humidity (2015–2017)	Humidity (+20%)
15	H-20	A decrease of 20% in the daily observed humidity (2015–2017)	Humidity (−20%)
16	DD0.5	Set up of the degree day coefficient (temperature at which snow melts) at 0.5 mm/°C/day	Melting rate of snow cover
17	DD4	Set up of the degree day coefficient (temperature at which snow melts) at 4 mm/°C/day	Melting rate of snow cover

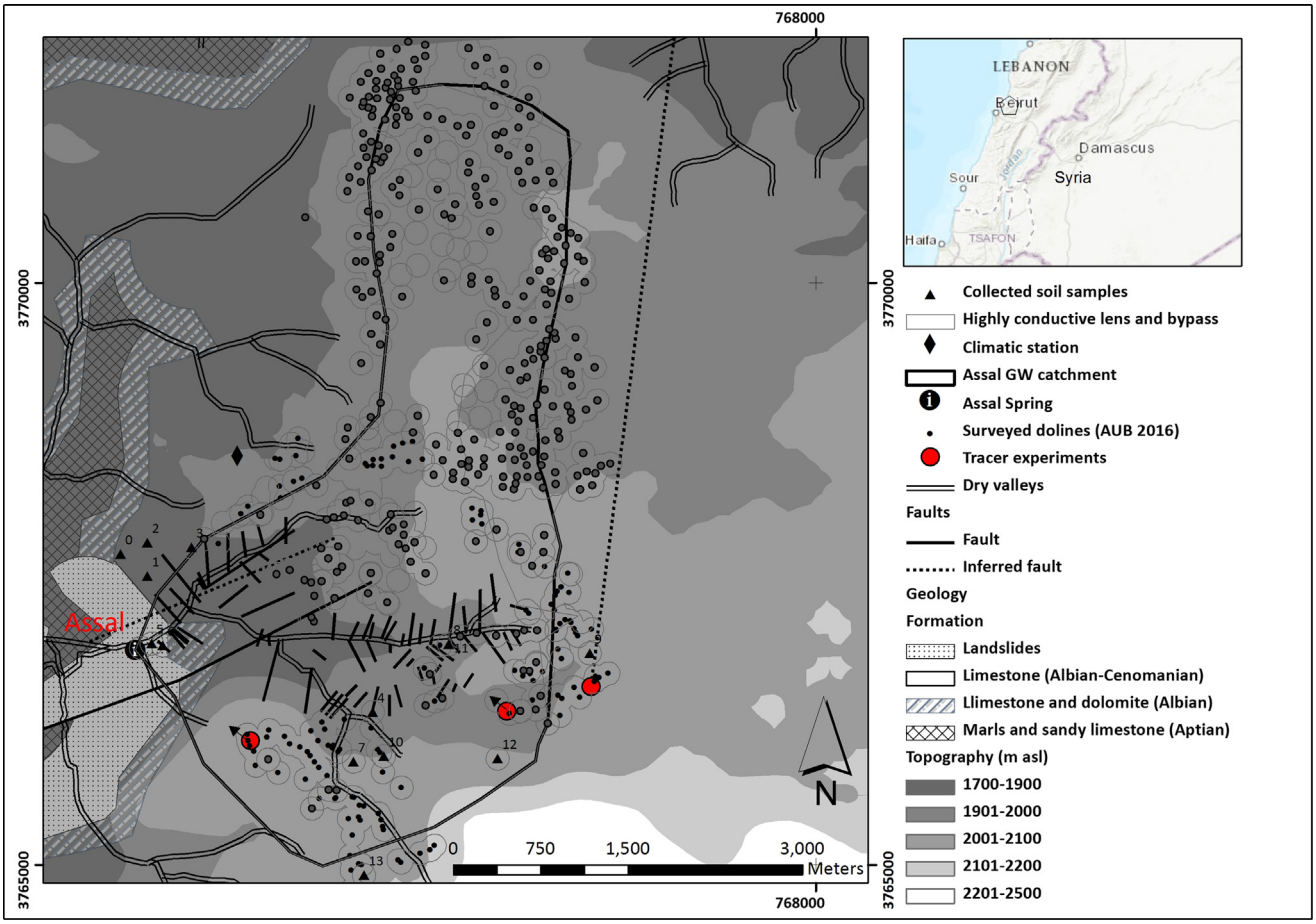

Fig. 2. Overview map of the field site showing the location of the Assal Spring in Mount Lebanon.

variation of temperature lies within the approximate range expected as future climatic models (Van Vuuren et al., 2011). Additionally, Lauffenburger et al. (2018) shows that an increase in temperature of 1 °C and 2.4 °C are expected in low and high warming scenarios respectively.

Scenarios 1 and 2 consist of a change in the precipitation daily values by an increase or decrease of 20% (Table 1). Scenarios 3, 4, and 5 represent variations (1, 3, and 8%) of the precipitation lapse rate (per change of 100 m altitude) with respect to calibrated value. The temperature varying scenarios included increasing and decreasing temperature time series by 2 °C (Scenarios 8 and 9), varying it by ± 20% (Scenarios 6 and 7), and changing the temperature lapse rate per 100 m equivalent to a change of ± 3% with respect to the temperature time series at an average elevation (Scenarios 10–11). Similarly, wind and humidity time series data points were increased and decreased by 20% in the calculations of potential evapotranspiration (Scenarios 12–15). Lastly, scenarios 16 and 17 vary the degree day coefficient. In this model, a simple degree day snow melt model based

Table 2
Parameterization of the integrated catchment hydrological model (MIKE She, 2016) and final calibration values.

Component		Parameters	Unit	Type of Data	Calibrated Value
Atmosphere and Surface	Climate data	Precipitation (P) Temperature (T) Ref. Evapotranspiration (ETP_r)	Mm	Daily time series elevation corrected	
	Snow melt	Melting temperature	°C	Constant	1
		Degree day coefficient	mm/°C/day	Constant	2
		Initial storage	Mm	Constant	0
	Vegetation (Kristensen and Jensen)	Leaf Area Index (LAI) Root Depth- (RD) Crop Coefficient (K_c)	– m	Seasonal time series/crop type distributed	
		C_1	–	Measured	0.2
		C_2	–		0.2
		C_3	mm/day		20
		A_{root}	–		0.25
		C_{int}	mm		0.05
Unsaturated Zone	Soil	Hydraulic Conductivity at saturation (K_s)	m/s	Measured/physical-Spatially distributed	1.22e−04
		Saturated moisture content (θ_s)	–		0.39
		Residual moisture content (θ_r)	–		0.176
		Alpha (α)	1/m		0.035
		n	–		1.75
		Bulk density	kg/cm^3		1600
		l (shape factor)	–		0.5
	Unsatura-ted rock matrix	Hydraulic Conductivity at saturation (Kuz_s)	m/s	Fitting	$10E^{-4}$
		Saturated moisture content (θuz_s)	–	Fitting	0.3
		Bubbling pressure (ψ_b)	m	Fitting	0.2
		Bulk density (ρuz)	kg/cm	Measured	2600
		Particle size index (λ)	–	Fitting	0.17
	Bypass	Bypass portion of net rainfall (BYP)	–	Spatially distributed (diffuse and point source; dolines)	0.25
		Moisture content for reduced bypass (BYPθ)	–		0.06
		Moisture content for no bypass (NOBYP)	–		0.05
Saturated Zone	Low conductive Matrix	Hydraulic conductivity (vertical and horizontal) (K_{xx}, K_{yy})	m/s	Measured	5.00e−05
		Specific yield (S_{yc})	–		0.1
		Specific Storage (S_{sm})	1/m		$10E^{-4}$
	Highly conductive zone	Hydraulic conductivity (vertical and horizontal) (K_x, K_y)	m/s	Fitting	0.3
		Specific yield (S_{yc})	–		0.1
		Specific Storage (S_{sc})	1/m		$10E^{-5}$
	Boundary conditions	Discharge rates (Q) (for Calibration)	m^3/s	Daily time series	

on an experimental average value of 6 mm/°C/day (Aouad-Rizk et al., 2005) is used to compute the amount of snow melt occurring daily.

For each sensitivity scenario, discharge time series were compared and contrasted to those of the calibrated spring to outline the sensitivity of the model to each of the climatic parameters. Additionally specific events such as spring responses to melting and spring recession that are characteristic of highly responsive karst catchments were selected for detailed analysis.

2.3. Future simulations using climate change scenarios

Precipitation, temperature, and radiation data for the years 2020–2099 were downloaded from the IPSL_CM5 GCM for Lebanon with a resolution of 0.25° based on the AgMERRA dataset (Ruane et al., 2015). The model "IPSL_CM5" (5th phase of the Coupled Model Intercomparison Project; J.L., Dufresne et al., 2013) was selected because of its ability to reproduce historical data for years 2014–2017 for the study area. The scenario RCP 6.0 was adopted; meaning a stabilization of the radiative forcing value without overshoot pathway at 6 W/m^2 after 2100 (Shrestha et al., 2016, Van Vuuren et al., 2011). Moreover, the projected raw daily output data was bias corrected (BC; Hawkins et al., 2013) using the differences in the mean and variability between GCM and observations in a reference period. The bias extracted corrected data were reflective of an elevation of 14 m above sea level, and thus do not account for the elevation of the catchment area (1500–2200 m). In order to correct for elevations, the raw historical data were compared and adjusted to the actual observation collected in the field for the years 2015–2017, using a calculated lapse rate for T (−0.24 °C) and P (+5.5%) per 100 m elevation. Based on an ensemble of 16 GCMs, the uncertainties associated with the climate parameters from the IPSL_CM5 GM may be on the order of ± 7% for low warming scenarios (RCP 2.6) and ± 20% for high warming scenarios (RCP 8.5) (Lauffenburger et al., 2018). Therefore, our use of the RCP 6.0 indicates that the uncertainties in climate parameters from the IPSL_CM5 GM are likely between ± 7% and ± 20%.

2.4. Data analysis

The input values were varied according to the 17 scenarios presented in Table 1, while the output functions were as follows: (1) total volume (Vt)/total recharge (R); (2) snow cover (SnC); (3) maximum (Q_{max}) and minimum flowrates (Q_{min}), (4) recession duration (Rec) since t(Q_{max}), (5) number of recession days (WS_d) where discharge falls below supply value (Q_s). Additionally, the sensitivity of the model to climate parameters was evaluated based on two objective functions: RMSE and a linear regression analysis between the calibrated daily discharge and the one retrieved from single sensitivity scenarios (R^2). The RMSE and R^2 of the calibrated scenario are considered 0 m^3/s and 1 respectively for the purpose of sensitivity analysis.

Standardization was applied to normalize the time series for comparison purposes by transforming the normally distributed output x_i to a new variable z_i that is also normally distributed.

The normalized time series were cross correlated using a Cross Correlation Function to determine the lag time (where the highest

Table 3
Selected results sensitivity analysis highlighting the effect of single climatic parameters on model output.

	Scenario	Selected results with respect to the calibrated scenario 0
1	P20	Decrease of the shortage period (WSd) by 8 days. Increase of maximum discharge by 0.32 m^3/s (+29%)
2	P-20	Lengthening of the shortage period (WSd) by 21 days. Decrease of maximum discharge by about 0.22 m^3/s (−21%)
3	Plapse1	Increase of the shortage period (WSd) by 14 days. Decrease of maximum discharge by 0.15 m^3/s (−13%)
4	Plapse3	Increase of the shortage period (WSd) by 11 days. Decrease of maximum discharge by 0.11 m^3/s (−10%)
5	Plapse8	Decrease of the shortage period (WSd) by 3 days. Increase of maximum discharge by about 0.14 m^3/s (+12%)
6	T20	Decrease of recession flow rate (13–27%)
7	T − 20	Increase of maximum flow rate (6–8%)
8	T + 2 °C	Respective declines of 0.035 and 0.14 m^3/s in the simulated minimum and maximum flowrates. Increase in the shortage period by 10 days
9	T − 2 °C	The discharge lags the calibrated discharge by 24 days, thus resulting in a decrease of the recession period and an increase in both recession and maximum flowrate (0.11 and 1.55 m^3/s respectively.
10	Tlapse-0.75	Decrease in recharge; recession coefficient increases to 0.023. Increase in maximum discharge by 24%. Recession flow rate decreases by 21%
11	Tlapse-0.15	Decrease in recharge; recession coefficient decreases to 0.013. Increase in maximum discharge by 3%. Recession flow rate decreases by 21%
12	W-20	Model is least sensitive to these parameters. ETR, Recharge,
13	W20	precipitation, recession coefficient and duration, maximum
14	H20	and minimum discharge and lag times remain unchanged
15	H-20	
16	DD0.5	a smoothening effect of the recession and decrease of the recession coefficient (0.003), allowing a considerable shortening of the recession period
17	DD4	a longer recession period by 32 days and a decrease in the recession flow rate to 0.09 m^3/s

correlation coefficient is obtained) between the simulated flowrates of the 17 scenarios (predictand) and the calibrated ones (predictor). The lag time represents the start of the recession period and the sensitivity of the tested parameter. The distribution and the significance of the data were evaluated using linear regression and hypothesis testing with an alpha (α) level of 0.05 (ANOVA and Tukey-Kramer tests).

For management purposes, water volume deficit and water shortage (WS) to be compensated during one hydrogeological year under various climatic scenarios can be calculated using the inferred recession coefficient and duration as (modified from Maillet 1905):

$$WS = 1-\left(\frac{V_a}{V_n}\right) = 1-\left(\frac{[\int_0^{WS_d} Q_s e^{-\alpha t}]}{Q_s WS_d}\right) \quad (5)$$

where V_n is the needed supply volume and V_a is the available spring volume, Q_s is the needed daily supply in m^3/d, WS_d is the duration of recession since t(Q_s) till end of hydrogeological year (Oct; in days), and α is the snow melt recession coefficient estimated for each scenario (1/d). Note that V_n and Q_s can be varied according to the increase of population and subsequent future demand.

3. Field site

El Assal karst spring is located at 1552 m (above sea level) in Mount Lebanon-Lebanon about 50 km from Beirut (Fig. 2). Its catchment area of about 12 km^2 was outlined based on five artificial tracer experiments (Fig. 2). The aquifer consists of three members of highly fissured, thinly layered basal dolostone overlain by dolomitic limestone and limestone of Albian to Cenomanian age. The spring emerges at the top of underlying marls and volcanics of Aptian age. The annual discharge of Assal spring is estimated at 15–22 Mm^3 (based on ongoing high-resolution monitoring since 2014). Dolines were mapped on the catchment area, and hydraulic properties of soil were estimated from representative samples collected on the catchment. Dolines and their characteristics were mapped on the catchment to determine zones of point source infiltration. Dry valleys are also considered fast flow pathways. The recharge area is located between 1600 m and 2200 m and is mostly dominated by snow melt. The spring provides downstream villages in the Kesrouane district with about 24,000 m^3 (0.28 m^3/s) of water daily for domestic use.

Table 4
Model results showing hydrograph characteristics (recession coefficients, maxima and minima) for selected simulated years along with fit objectives results. (RMSE: Residual Mean Square Error).

	Year	2014–2015	2015–2016	Average (2013–2017) including one dry year
Input data	Precipitation; P (mm)	1931	1349	1370
	Max temperature (T_{max})	33.56	27.29	27.54
	Min temperature (T_{min})	−6.13	−5.82	−5.73
	Potential Evapotranspiraion ETP_{ref} (mm)	536	624	612
Model results	Snow cover (SnC)	630	462	
	Real Evapotranspiration; ETR (mm)	228	226	218
	Recharge; R (mm)	1681	1157	1148
	Annual olume (mm)	1633	1157	1144
	ETR/P (%)	12%	17%	16%
	R/P (%)	87%	86%	84%
	Annual volume/P (%)	85%	86%	84%
	Recession coefficient (1/d)	0.018	0.018	0.018–0.022
	Recession flowrate (m^3/s)	0.10	0.07	0.10
	Maximum discharge (m^3/s)	1.7	1.5	1.46
Observed data	Annual Volume (mm)	1481	1005	900
	Recession flowrate (m^3/s)	0.1	0.1	0.1
	Maximum discharge (m^3/s)	2	2	2.5
	Recession coefficient (1/d)	0.023	0.018	0.022
	Recession flowrate (mm)	0.7	0.5	0.7
	Maximum Discharge (mm)	10.3	9.40	15.5
Fit	RMSE (m^3/s)	0.26	0.21	0.28
	R^2 (Nash-sutcliffe)	0.77	0.78	0.62
	Maximum error in volume (%)	10%	15%	21%

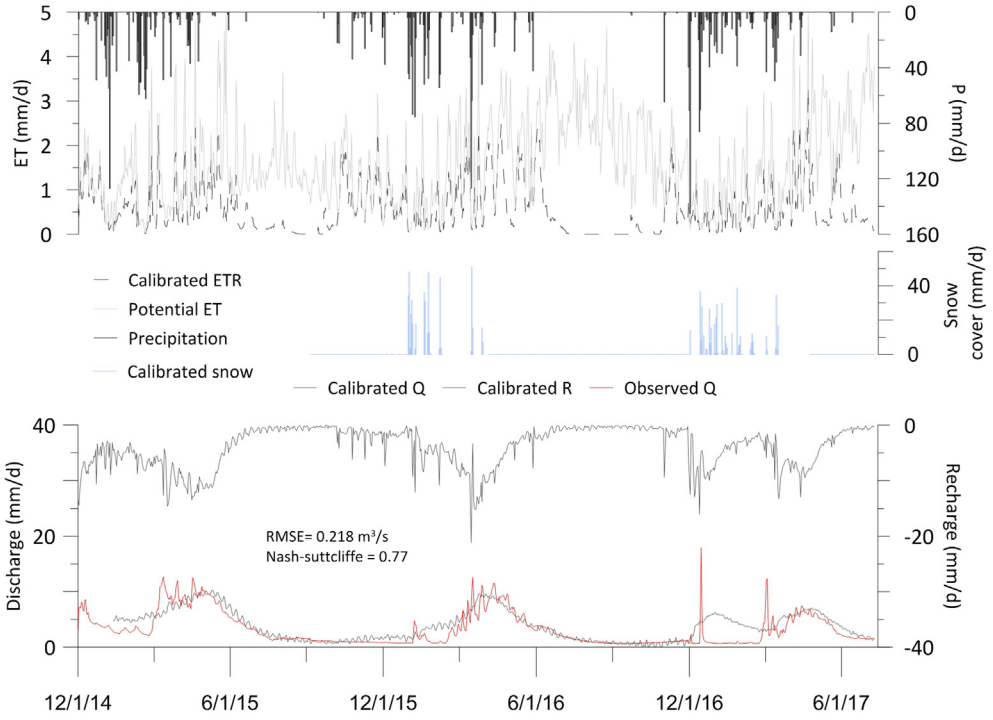

Fig. 3. Calibrated spring responses to precipitation including real evapotranspiration, snow, recharge, and discharge for the years (2014–2017).

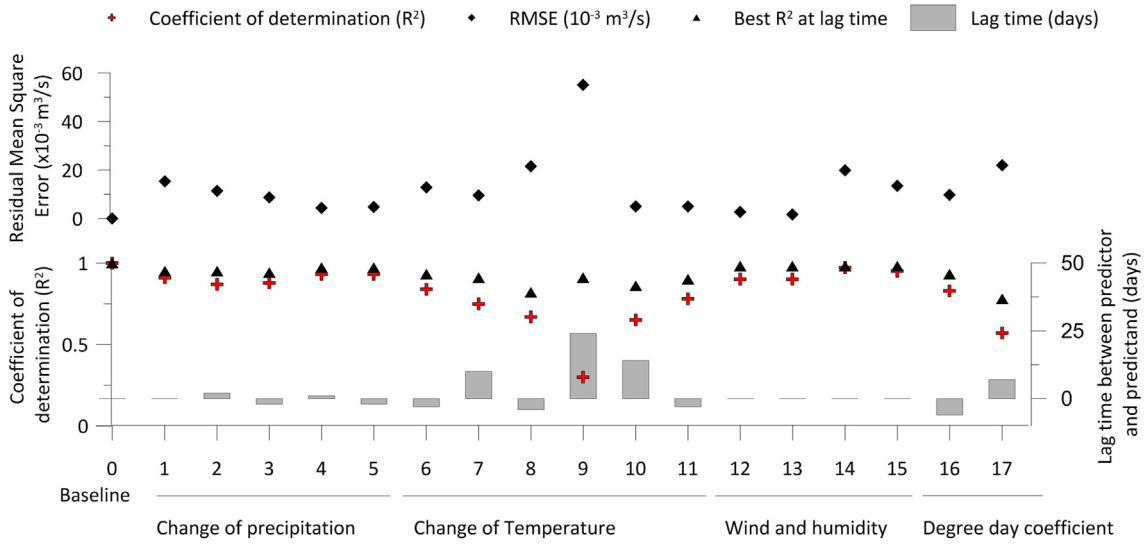

Fig. 4. Residual Mean Square error (m^3/s) and coefficient of determination (R^2) between the calibrated discharge (Q_{cal}) and the one (Q_{sens}) extracted from the sensitivity analysis simulations upon variation of single climatic parameters. The lag time refers to lag time at which the discharge Qsens and Qcal time series are best correlated (based on a cross correlation function).

4. Results and discussion

4.1. Model results

The observed hydrographs (2013–2017) were successfully simulated with the integrated spatially distributed model. The calibrated parameters used in the model in the three compartments are shown in Table 2. Selected results of the single parameter sensitivity analysis are highlighted in Table 3

Results in Table 4 and Fig. 3 show that the RMSE of 0.218 m^3/s lies within the recession discharge of the spring. The E of 0.77 implies a satisfactory fit for the purpose of this work. It is to be noted that in the simulated discharge peaks are not well reproduced with respect to the flowrates of the recession period. The latter is due to the duality of the flow components (fast versus slow) that are represented with a single continuum model with varying hydraulic conductivities and thus resulting in the inability of the model to reproduce the fast flow component to a certain level of precision. The total precipitation (including rain and snow) ranges between 1350 mm and 1950 mm. Reference evapotranspiration was calculated to be about 500–600 mm, however most of the real evapotranspiration (ETR) occurs during the summer period where there is no availability of water for evapotranspiration. The latter explains the relatively low amount of real evapotranspiration (between 12 and 15% of the total budget), which is similar to values obtained for this region by Hartmann et al. (2014). Surface runoff is considered negligible as it occurs for a maximum of 7 days during the

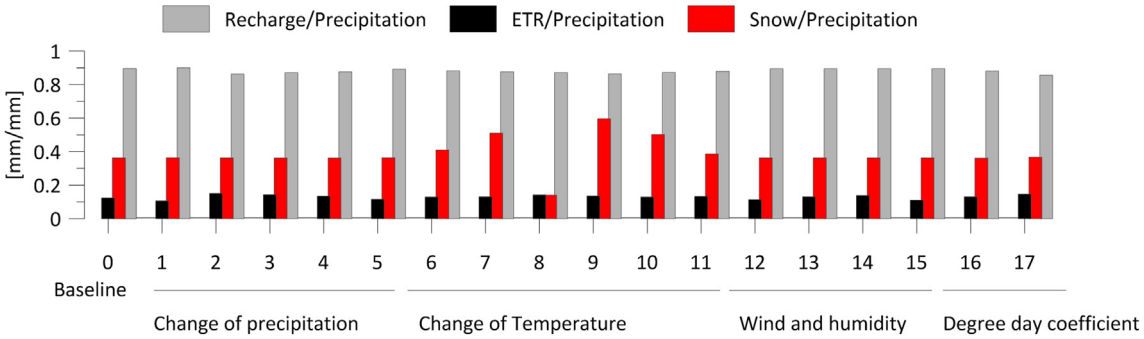

Fig. 5. Ratio of ETR, Snow, and Recharge to precipitation for each of the climatic sensitivity scenarios.

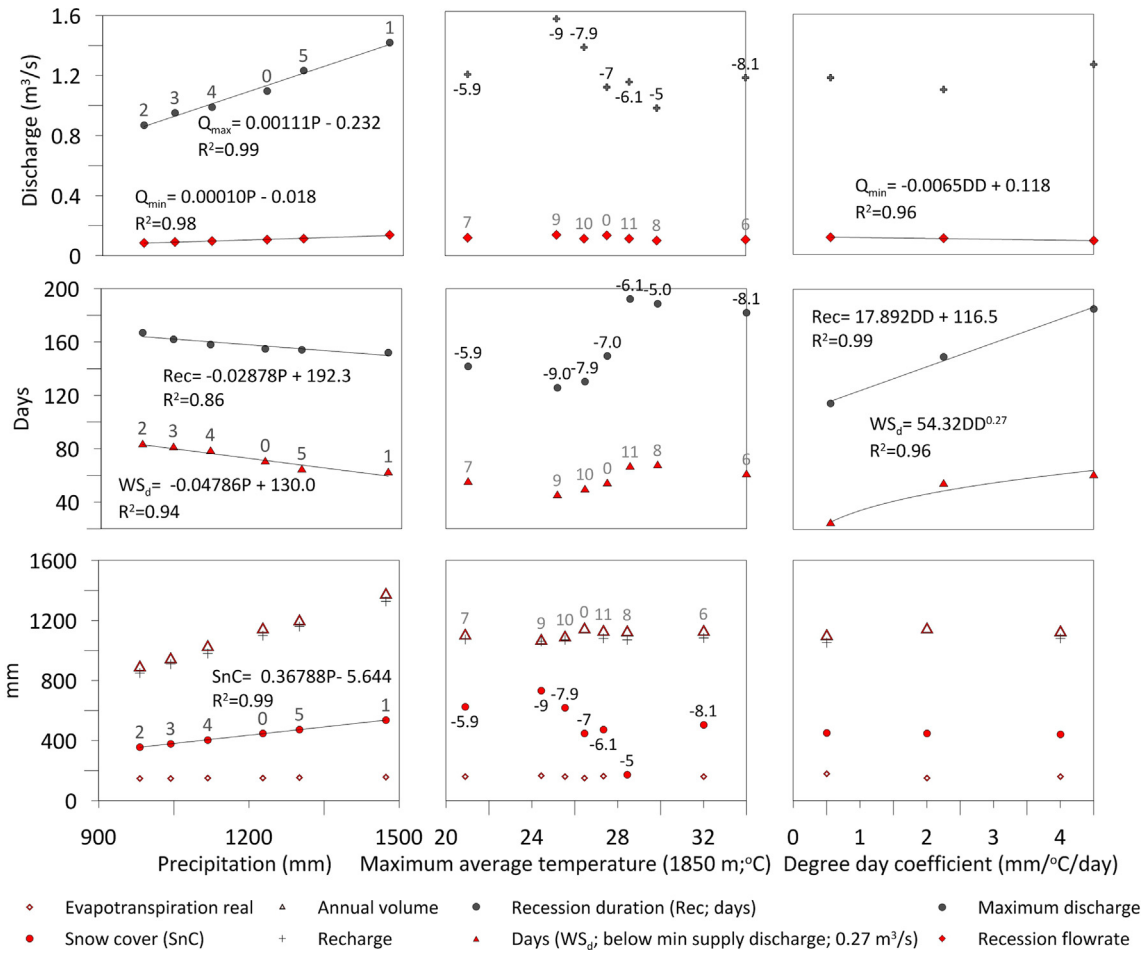

Fig. 6. Variation of the model response to a variation in single climatic input: Impact on recession, flowrates and annual volumes. Labels in grey refer to scenario number and black labels refer to minimum temperature in ˚C observed on the catchment.

hydrological year only in the dry valleys. The total simulated cumulative recharge on the catchment ranges between 84 and 85% of the total precipitation, which is considered relatively high, but very comparable to recharge rates in well-developed karst systems with significant point source infiltration under semi-arid conditions (Hartmann et al., 2014; Nikolaidis et al., 2013). The calibrated recharge and discharge are well correlated together with a lag of 14 days between recharge and discharge (R^2 = 0.882).

4.2. Single parameter sensitivity analysis

Single parameter sensitivity revealed the impact of temperature (T) and precipitation (P) along with other model parameters such as wind, humidity, and rate of snow melt per change of temperature. The effect of each parameter is evaluated based on the RMSE and the coefficient of determination (R^2) between the calibrated discharge rates (Q_{cal}) and the sensitivity analysis ones (Q_{sens}) (Fig. 4). With a ratio of ETR to P ranging between 0.1 and 0.15, the ratio of recharge to precipitation varies between 0.85 and 0.9 in all the sensitivity scenarios. Moreover, the ratio of snow to precipitation remains invariant except in temperature scenarios 6–11. e.g., it decreases from 0.36 in baseline scenario to 0.14 in scenario 8 (Fig. 5).

4.2.1. Effect of precipitation (Scenarios 1–5)

The change of precipitation rates results in a maximum RMSE of 0.011–0.015 m^3/s with a coefficient of determination of 0.87–0.91

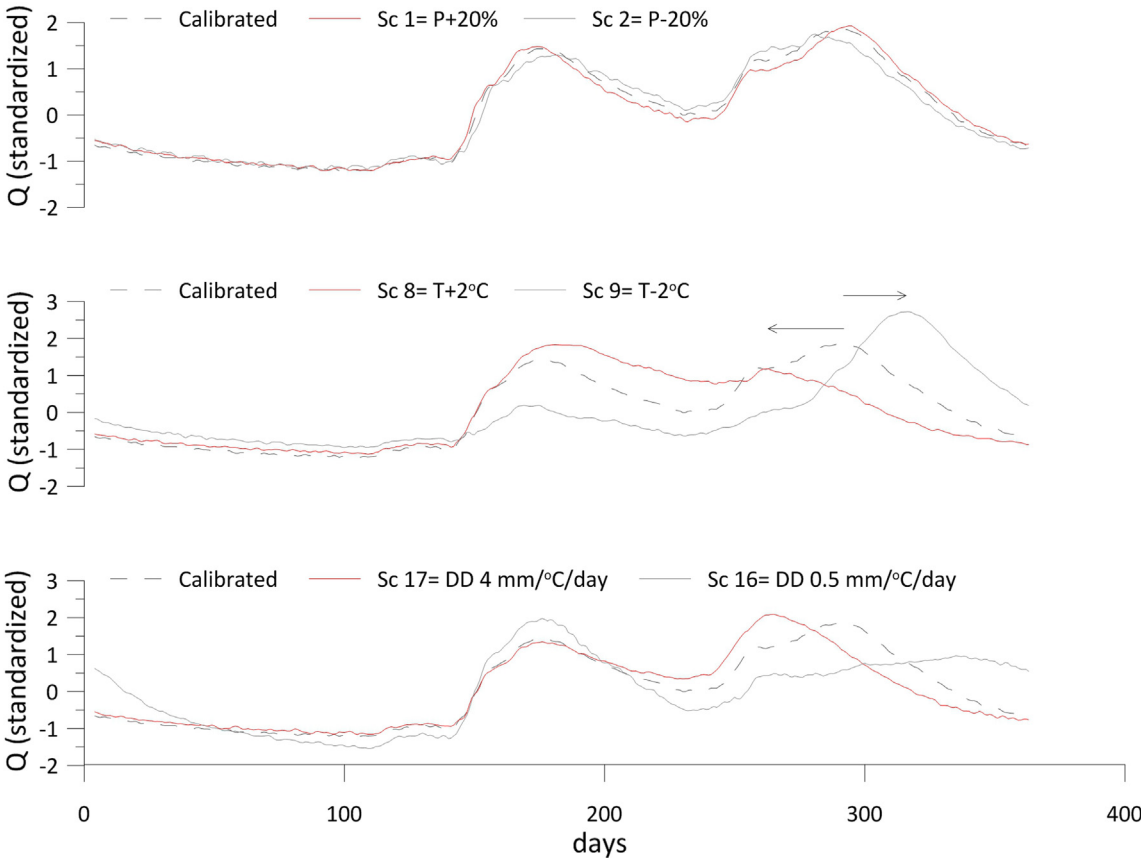

Fig. 7. Lags observed between standardized discharge rates obtained in selected sensitivity scenarios in comparison to the calibrated discharge (0 = July 2016).

(Fig. 4). The increase in precipitation leads to the linear increase of annual snow cover, recharge, and annual volume of the spring, along with maximum and minimum discharge according to the trends shown in Fig. 6. Generally, the number of recession days decreases linearly by −0.03 day/mm and the recession flow rate increases by 0.0001 $m^3/s/mm$ with increasing annual precipitation (Fig. 6).

The recession coefficient increases slightly (0.014–0.019) with increasing precipitation, which indicates a relatively faster recession slope, and a higher input from fast flow pathways. Additionally, an increase of precipitation by about 20% will result in the decrease of the shortage period (WS_d) by 8 days, while a 20% decrease in precipitation will lead to its lengthening by 21 days as illustrated by the lags observed in the standardized sensitivity time series with respect to the calibrated one (Fig. 7).

The real evapotranspiration (ETR) appears to remain relatively constant (Fig. 6), even with increasing precipitation, which is a result that agrees with Hartmann et al., 2014. Additionally, the ratio of recharge to precipitation increases with higher precipitation amounts (Fig. 5).

The lapse rate for precipitation (Plapse) was varied around the value of 6 mm per 100 m: 1, 3, and 8 to test the effect of the change of the precipitation amount with elevation on model results (Table 1; Fig. 6). In future climatic models, a decrease of the precipitation lapse rate (Scenarios 3 and 4) is to be anticipated with an intensified warming rate in altitude (Isotta et al., 2014; Mountain Research Initiative EDW Working Group, 2015), leading to a decrease of total precipitation amounts. Under these conditions, the variation of recharge, spring volume and discharge maximum and minimum can be quantified using a linear relationship as well (Fig. 6; Scenarios 3 and 4).

4.2.2. Effect of temperature

The decrease of the daily temperature values by 2 °C, results in a maximum RMSE of 0.06 m^3/s and a R^2 of 0.30 (Fig. 4; scenario 9). The variation of both minimum and maximum temperature yields variable impacts on snow cover, but has little effect on annual recharge and volume (Fig. 6). Model results show that the variation of temperature within the 5 scenarios ranges have a little effect on ETR (not exceeding 15%). The discharge obtained in scenario 9 lags the calibrated discharge by 24 days, thus resulting in a decrease of the recession period and an increase in both recession and maximum flowrate (Fig. 7). Contrarily in scenario 8, an increase of temperature by 2 °C yields an increase in the shortage period by 10 days (Fig. 7).

4.2.3. Effect of wind and humidity

A change of 20% in humidity and wind speed (Scenarios 12 and 13) in the model revealed to have minimal influence on the recharge and discharge signals (Figs. 3 and 4). As shown in Fig. 5, the change of wind and humidity impact cumulative reference evapotranspiration (ETP_{ref}) and the ratio of total ETR/P. For example, an increase of wind speed by 20% leads to a decrease in total ETR (−7%), while a change in humidity by ± 20% inversely affects total ETR (± 11%).

4.2.4. Effect of degree day coefficient

However, an increase of this factor (Scenario 17) is expected in future climatic scenarios according to snow degree day models (Bliss et al., 2014; Yang et al., 2014). Therefore, accelerated snow melt yields as expected (Scenario 17), a longer recession period and a decrease in the recession flow rate (Figs. 6; 7). However, compared to P and T, this parameter has a less significant effect on total volumes (discharge, recharge or snow cover; Fig. 6). A decrease in the degree day coefficient (0.5 mm/°C/day) (Scenario 16) will result in a smoothening effect of the recession and decrease of the recession coefficient, allowing a considerable shortening of the recession period (Fig. 7).

The single parameter sensitivity analysis shows that temperature

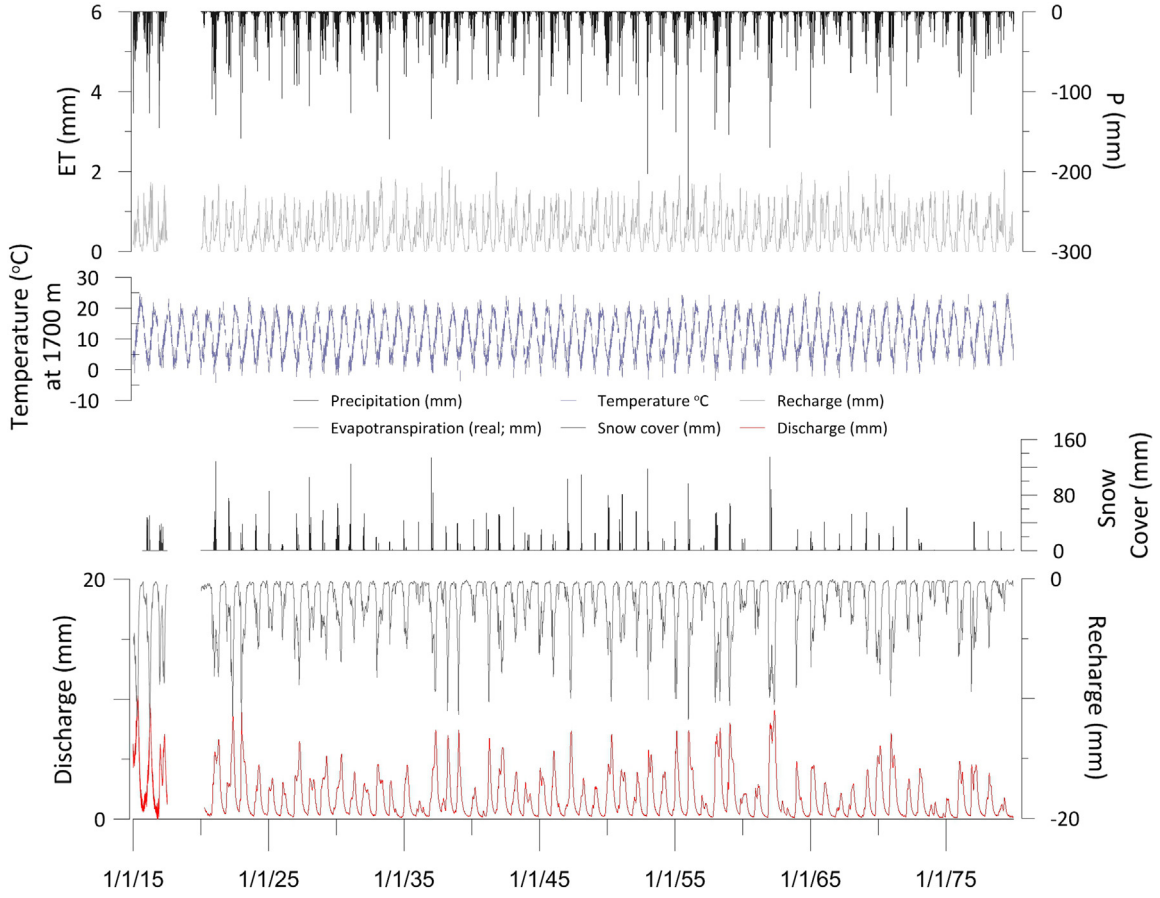

Fig. 8. Output model parameters for future climatic scenario simulation (IPSL_CM5/RCP 6.0) from 2015 to 2080

plays the most significant role in the discharge output (highest RMSE and lowest R^2 when compared with the calibrated series). Temperature is significant because it greatly affects recession parameters, volumes, and the shape of the time series. An increase of a minimum of 2 °C as predicted by climatic scenarios (Shrestha et al., 2016) leads to an exponential lengthening of the recession period and flowrate and to a substantial decrease in snow cover, while the effect on annual recharge/annual spring volumes remains less significant. Any increase in temperature will eventually translate into longer shortage periods with subsequent lower recession flowrates. For instance, an urgent need to seek alternative resources (up to 77% of the needed supply volumes) arises with an increase of 2 °C in T.

4.3. Climate change model results

The trends of the model signals (precipitation, ETR, maximum and minimum temperatures, snow, recharge, discharge rate; Fig. 8) between years 2020 and 2099 were evaluated to estimate the expected change in the model as a response of future projected precipitation and temperatures.

A Shapiro-Wilk test for normality that was run on precipitation, ETP, recharge, and discharge indicate that the data are drawn from a non-normal population (p-values $< \alpha = 0.05$). Spearman's ρ indicate a statistically significant (p-value < 0.0001) a moderate ($\rho = 0.33$) positive correlation between precipitation and recharge, and a strong (p-value < 0.0001, $\rho = 0.88$) positive correlation between recharge and spring discharge.

The linear regression models for each of precipitation, ETP, recharge and discharge are statistically significant (p-values < 0.05), indicating temporal trends with each of these variables over the 21st century. Linear regressions for model outputs are characterized by low R^2 indicating that linear trends could only explain little variance (0.03–1.18%) in precipitation, real evapotranspiration (ETR), recharge and discharge over the entire time domain (2020–2099; Fig. 9). Nevertheless, the trend indicates that precipitation time series decreases with a slope of −2.33 mm/y, while ETP increases at a moderate rate of 0.22 mm/year (Fig. 9). Moreover, with an increase of minimum and maximum temperature of 0.03 °C per year, snow cover is expected to decline at a rate of 3.1 mm/y. Additionally, the trend of recharge is −2.6 mm/year coupled with a decrease of the spring annual volume at a rate of 38,300 m^3/y (equivalent to 12 l/s/y). The expected maximum discharge decreases as well, at a yearly rate of 0.003 m^3/s (3 l/s).

To further evaluate the temporal trends in discharge and recharge, the data series were divided into intervals of 25-year periods (2020–2044, 2045–2069, and 2070–2099). Results of an ANOVA test indicate that there are statistical differences (p-value < 0.0001) in the mean values of recharge and discharge in the three time periods. The Tukey-Kramer test indicate that mean rates of recharge and discharge are not statistically different between 2020 and 2044 and 2045–2069, but are statistically lower by the final third of the 21st century (2070–2099).

Moreover, all the output signals time series were also evaluated in 10-year interval to depict outliers and varying trends in the future (Fig. 10). In concordance with the Tukey-Kramer test, starting year 2070, decreasing precipitation varying around a mean average of 800 mm, leads to a drastic decline of recharge and annual volume at the spring (Fig. 10). After 2070, recharge and discharge rates are less than 50% of the rates prior to 2070 (Fig. 10). Similarly to this study, Hartmann et al. (2012) shows that after 2068, flowrates of a simulated karst Mediterranean spring start portraying considerable variabilities.

The significant decline in recharge and discharge by the end of the 21st century is driven by mostly positive temperatures all year long,

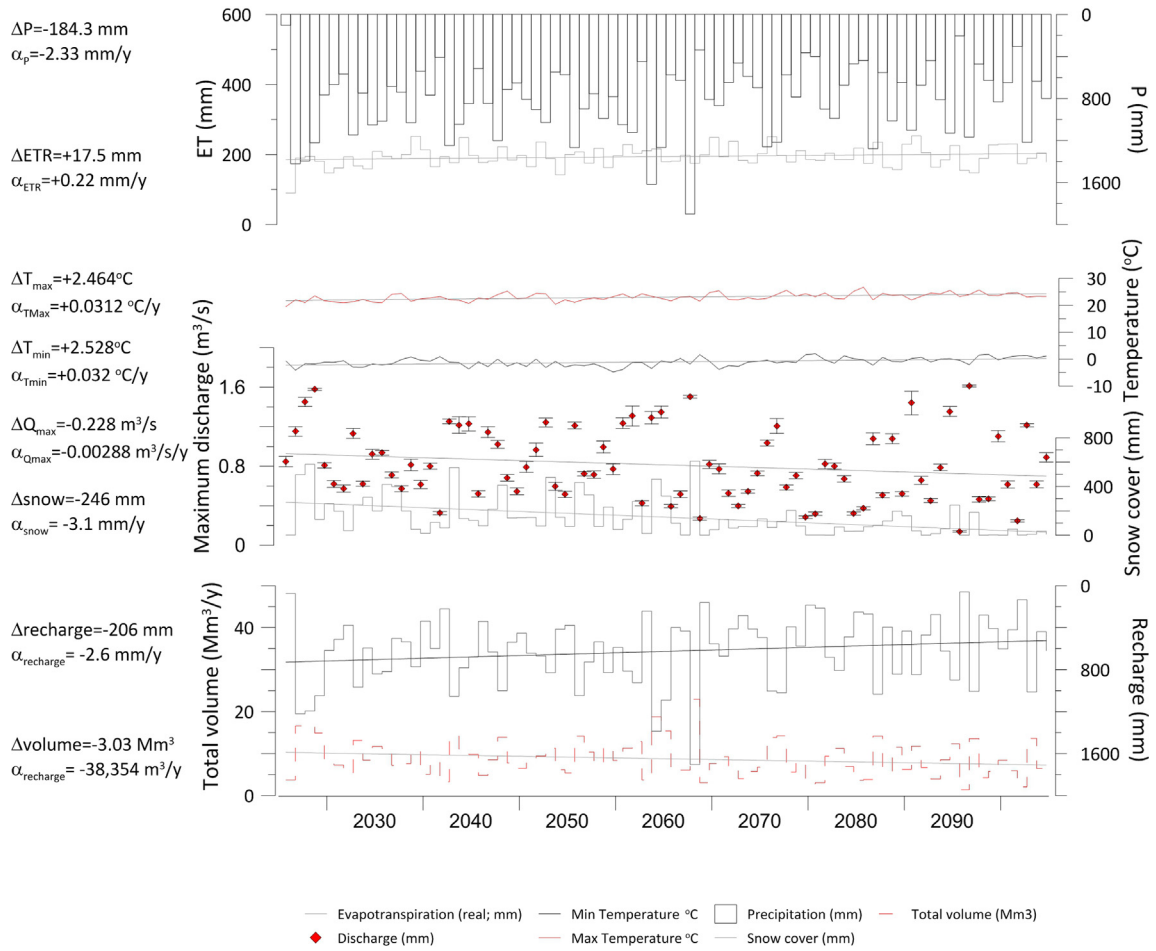

Fig. 9. Total annual values of ETR, snow cover, recharge, and spring volumes, in addition to average air temperature maxima and minima and spring maximum flowrates expected from 2020 to 2099 based on the simulated model using corrected IPSCMP_5 model for the area. Delta (Δ) represents the total difference in the output and alpha (α) is the average trend between present and final values in 2100.

leading to the decrease of snow cover to nil. Maximum discharges and minimum flowrates at the springs are projected to reach as low as 0.24–0.5 m^3/s and 0.012–0.016 m^3/s, respectively with annual spring volumes dropping to 0.37–5.00 Mm^3, equivalent to about 20% drop with respect to current status. Based on simulations of an ensemble of 50 climate change models, water availability in a Mediterranean karst is expected to decrease by a similar range 15–30% (Hartmann et al., 2012). Recession coefficients vary between 0.014 and 0.025 (1/d) indicative of conduit and fissured matrix storage (Baedke and Krothe, 2001). The length of the recession period increases at an overall rate of 0.55 day/year, while the shortage in supply volume (WS) during recession can reach up to 65% to be supplied by alternative means. It varies from a minimum of 131 days (year 2030) to about 291 days (year 2071 and 2091) corresponding to 4.5–10 months in comparison to the calibrated year 155 days; 5 months). Its duration is moderately correlated with snow cover, especially in the years 2020–2069 (Fig. 11). After year 2070, snow cover decreases to below 200 mm, where the length recession period becomes majorly controlled by minimum temperature (a minimum of −2.25 °C; Fig. 10). With increasing temperature, rapid infiltration of snowmelt into fast preferential pathways is highly reflected in rapid increase of discharge and indirectly impacts the duration and time of recession (Geyer et al., 2008). Chen et al. (2017) shows that the spatial-temporal distribution of discharge under snow governed aquifers is highly dependent on temperature variation, because of snow storage decline under varying climatic scenarios.

The forward simulation of the model using future climate projections allows identifying wet and dry years and the quantitative impact of extreme climatic conditions on the spring. Therefore, model results for selected years (average, wet year (P > 1000 mm), dry year (P < 500 mm), and extremely dry year (P < 400 mm) were also compared and contrasted to those of 2015 (Table 5) to evaluate the spring response to unusual hydrogeological years. In extremely dry and dry years, snow cover decreases to 1–77 mm, and the recharge to precipitation ratio drops to 0.5 (e.g., 2073–2074). Notwithstanding the decrease in total ETR during dry years, real evapotranspiration makes up to 50% of the total precipitation. Similarly, an increase of 15–25% in evapotranspiration is expected with a decrease of 53–98% in recharge (Lauffenburger et al., 2018) under different global warming scenarios. Wet years results (e.g., 2036–2037) are comparable to the calibrated model of year 2015–2016, while in forthcoming average years (e.g., 2034–2035) with decreasing annual discharge volumes, snow cover, and recharge to precipitation ratio, an earlier recession is to be expected (Table 5). The lag time between the recharge and discharge signals increases slightly during wet periods and decreases during drought periods mostly due to the decrease of snow cover and melt, which makes the spring highly responsive to rain events (higher maxima) and subsequently running dry early during recession (Q below 0.001 m^3/s). The latter is highly dependent on an increasing minimum temperature coupled with decreasing temperature (Table 5).

5. Conclusions

A calibrated integrated spatially distributed hydrological model of a karst catchment in semi-arid conditions (Lebanon) was used to perform

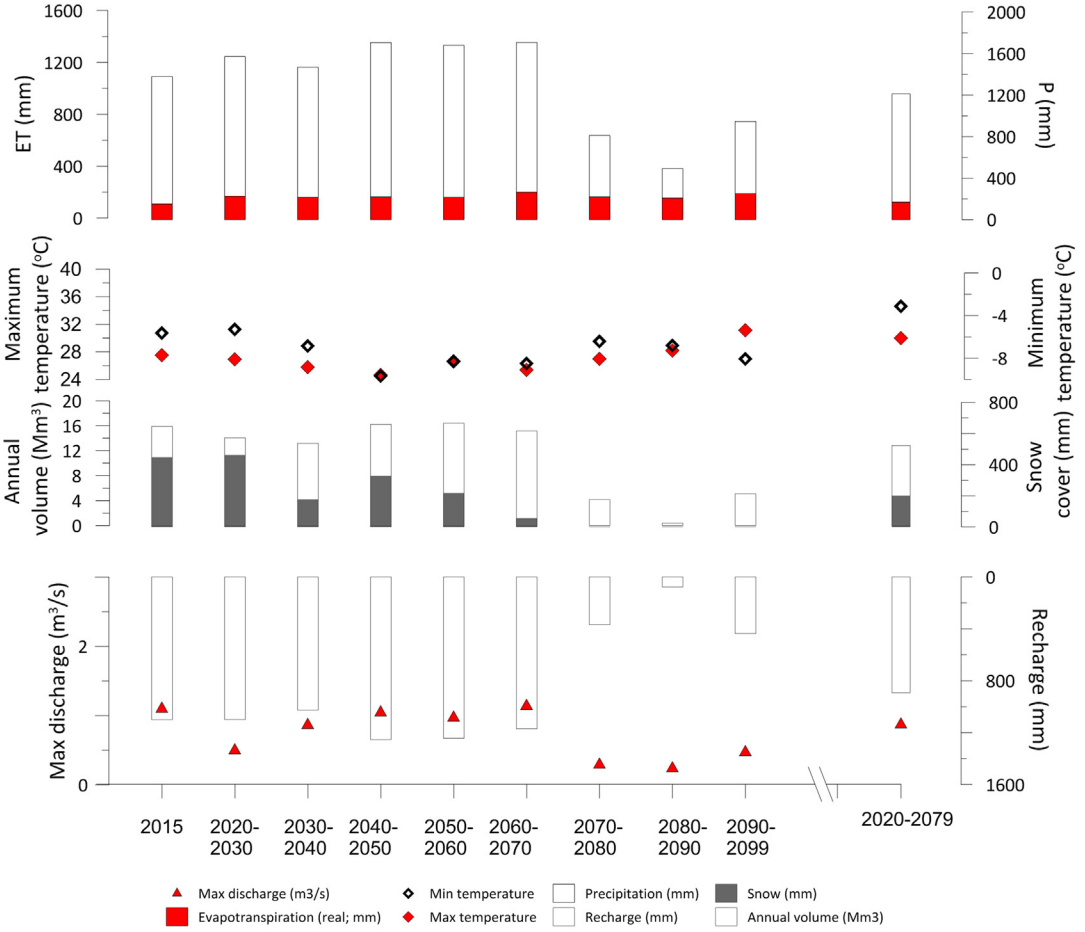

Fig. 10. Average values of model signals over a 10-year interval between 2020 and 2099 in comparison to 2014–2015

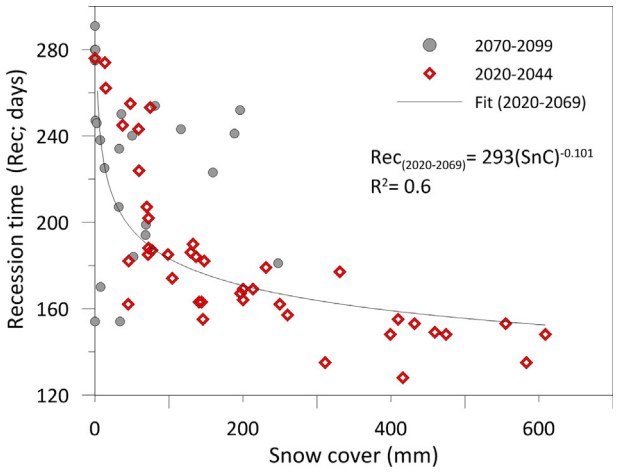

Fig. 11. Relationship between yearly snow cover (mm) and recession period (days) from 2020 to 2069 and 2070–2090.

sensitivity analysis on single climate parameters and to simulate future spring responses to a projected climate scenario for the 21st century. Temperature appears to be most important parameter that significantly impacts model output and results, especially snow cover, flow minimum and maximum, as well as the duration of recession period, while having little effect on total spring volumes. The variation in precipitation yields a linear variation in all model output. Real evapotranspiration (ETR) constitutes between 12 and 18% of the overall water budget and remains relatively constant in the 17 single parameter sensitivity scenarios. Other parameters such as increasing degree day coefficient have considerable effect on enhancing snow cover melting and subsequent increase in recession duration.

The forward simulation using daily downscaled climatic P and T data (model IPSL_CM5 scenario RCP 6.0) shows that recharge and discharge are highly correlated together and time-dependent. Snow cover is the most affected hydrological parameter because of critical increasing temperature above snow freezing/melting point in the region. As a result, the recession duration is expected to increase at a rate of 0.55 day/year. The decreasing snow accumulation will lead to a more prominent flushing of precipitation event waters into fast preferential pathways, thus increasing discharge magnitude at the spring over short periods of times. Moreover, as a response to the predicted temporal trends in precipitation and temperature, negative trends are expected to occur in recharge and annual spring volumes, with a negligible increase in ETR, especially starting around the year 2070. The response of the spring to a less significant snow cover and melt will be clearly evident in the decreasing flowrate maxima, and a lengthening of the recession period and its early arrival (30 days with respect to current situation). Finally, this study quantified the effect of a changing climate for the region on spring output such as (1) spring volume or annual recharge rates, (2) recession coefficient and duration, (3) maximum and minimum flowrate, (4) variation of snow cover, and (5) deficit volume below demand rate during shortage periods, which constitute key parameters in groundwater management and decision making. Therefore the model results could be up-scaled on other similar catchments and snow-melt driven water supplies in Lebanon or in semi-arid climates of the greater Mediterranean region. Additionally, findings from this study allow decision makers to implement best informed

Table 5
Water budget analysis for selected exceptional years (average, wet, dry and extremely dry) in comparison to that of the calibrated year 2015–2016 (R^2 stands for coefficient of determination).

	Year	(2015–2016)	Average year (2034–2035)	Wet year (2036–2037 P > 1000 mm)	Dry year (2039–2040 P < 500 mm)	Extreme dry year (2073–2074) P < 400 mm
Input data	Precipitation; P (mm)	1349	767	1246	513	362
	Max temperature (T_{max})	27.29	29.0	28.3	29.0	24.29
	Min temperature (T_{min})	−5.82	−0.8	−1.2	−1.00	1.6
	Potential Evapotranspiraion ETP_{ref} (mm)	624	656	654	665	699
Model results	Snow cover (SnC)	442	104	555	77	0.97
	Real Evapotranspiration; ETR (mm)	226	165	176	177	186
	Recharge; R (mm)	1157	597	1027	339	185
	Annual volume (mm)	1157	586	1054	350	196
	Annual volume (Mm^3)	16.4	8.16	14.14	5.00	2.79
	ETR/P (%)	17%	22%	14%	35%	50%
	R/P (%)	86%	78%	82%	66%	50%
	Annual Volume/P (%)	86%	76%	85%	68%	54%
	Start of recession period	2-May	9-Apr	3-May	1-Apr	3-Mar
	Recession coefficient (1/d)	0.018	0.011	0.022	0.021	0.021
	Recession flowrate (m^3/s)	0.07	0.04	0.06	0.001	0.001
	Maximum discharge (m^3/s)	1.52	0.72	1.45	0.52	0.28
	Recession period (Rec, days)	155	175	152	186	204
Cross correlations	Error (mm)	3.8	3.9	1.9	6.3	4.8
	R^2 with Q (2015–2016)	1.00	0.33	0.85	0.54	0.22
	Lag (days) between R and Q	14	16	16	8	8
	Best R^2 at lag time	0.88	0.84	0.91	0.72	0.69
	Change in Volume (%)	0%	−50%	−14%	−70%	−83%

practices for long term water resources planning and management, especially in complex karst systems, to overcome the impacts of climate change on water availability. These practices may include finding alternative resources or investigate or implement managed aquifer recharge in the case of water exceedance during the high flow period to increase the storage capacity.

Acknowledgement

This work was funded by a USAID PEER Science project Award number (102881; Cycle 3). The authors would also like to thank Fouad Andari and Michel Aoun for their help during fieldwork. The kind support of Engineers George El Kadi and Joseph Nseir Beirut from Mount Lebanon Water Establishment and that of Kfarzebian municipality is highly appreciated.

References

Andreo, B., Vıas, J., Duran, J.J., Jimenez, P., Lopez-Geta, J.A., Carrasco, F., 2008. Methodologies for groundwater recharge assessment in carbonate aquifers: application to pilot sites in southern Spain. Hydrogeol. J. 16 (5), 911–925.

Aouad-Rizk, A., Job, J.-O., Khalil, S., Touma, T., Bitar, C., Boqcuillon, C., Najem, W., 2005. Snow in Lebanon: a preliminary study of snow cover over Mount Lebanon and a simple snowmelt model. Hydrolog. Sci. J. 50 (3), 569.

Baedke, S.J., Krothe, N.C., 2001. Derivation of effective hydraulic parameters of a karst aquifer from discharge hydrograph analysis. Water Resour. Res. 37 (1), 13–19.

Bates, B.C., Kundzewicz, Z.W., Wu, S., Palutikof, J.P. (Eds.), 2008. Climate Change and Water. International Panel on Climate Change (IPCC) Secretariat, Geneva Technical Paper.

Beniston, M., Stoffel, M., 2016. Rain-on-snow events, floods and climate change in the Alps: events may increase with warming up to 4°C and decrease thereafter. Sci. Total Environ. 571, 228–236.

Birk, S., Liedl, R., Sauter, M., 2004. Identification of localized recharge and conduit flow by combined analysis of hydraulic and physicochemical spring responses (Urenbrunnen, SW-Germany). J. Hydrol. 286, 179–193.

Bliss, A., Hock, R., Radić, V., 2014. Global response of glacier runoff to twenty-first century climate change. J. Geophys. Res. Earth Surf. 119, 717–730.

Butscher, C., Huggenberger, P., 2009. Modeling the temporal variability of karst groundwater vulnerability with implications for climate change. Environ. Sci. Technol. 43, 1665–1669.

Charlier, J.P., Ladouche, B., Maréchal, J.C., 2015. Identifying the impact of climate and anthropic pressures on karst aquifers using wavelet analysis. J. Hydrol. 523, 610–623.

Chen, Z., Hartmann, A., Wagener, T., Goldscheider, N., 2017. Dynamics of water fluxes and storages in an Alpine karst catchment under current and potential future climate conditions. Hydrol Earth Syst. Sci. Discuss. https://doi.org/10.5194/hess-2017-216.

Christensen, J.H., 2007. Regional climate projections, in climate change 2007: the physical science basis. In: In: Solomon, S. (Ed.), Contribution of Working Group I to the Fourth Assessment Report of the Intergovernmental Panel on Climate Change Univ. Press, Cambridge, UK.

Dar, F.A., Perrin, J., Ahmed, S., Narayana, A.C., Riotte, J., 2014. Hydrogeochemical characteristics of Karst Aquifer from a semi-arid region of Southern India and impact of rainfall recharge on groundwater chemistry. Arab. J. Geosci. 8 (5), 2739–2750.

Denmark Hydrology Institute (DHI), 2016. Mike She User Manual and Reference Guide, December 2007, Denmark (V1 and 2).

Doummar, J., Sauter, M., Geyer, T., 2012. Simulation of flow processes in a large scale karst system with an integrated catchment model (Mike She) – Identification of relevant parameters influencing spring discharge. J. Hydrol. 426–427, 112–123.

Dufresne, J.L., Foujols, M.A., Denvil, S., et al., 2013. Climate change projections using the IPSL-CM5 Earth System Model: from CMIP3 to CMIP5. Clim Dyn. 40, 2123.

Giorgi, F., Lionello, P., 2008. Climate change projections for the Mediterranean region. Glob. Planet. Chang. 63, 90–104.

Geyer, T., Steffen Birk, S., Rudolf Liedl, R., Sauter, M., 2008. Quantification of temporal distribution of recharge in karst systems from spring hydrographs. J. Hydrol. 348 (3–4), 452–463.

Gleeson, T., Wada, Y., Bierkens, M.F., van Beek, L.P., 2012. Water balance of global aquifers revealed by groundwater footprint. Nature 488, 197–200. https://doi.org/10.1038/nature11295.

Goderniaux, P., Brouyère, S., Wildemeersch, S., Therrien, R., Dassargues, A., 2015. Uncertainty of climate change impact on groundwater reserves – application to a chalk aquifer. J. Hydrol. 528, 108–121.

Green, T., Taniguchi, M., Kooi, H., Gurdak, J.J., Hiscock, K., Allen, D., Treidel, H., Aurelia, A., 2011. Beneath the surface of global change: Impacts of climate change on groundwater. J. Hydrol. 405, 532–560. https://doi.org/10.1016/j.jhydrol2011.05.002.

Gurdak, J., 2017. Climate-change impacts, developing world, Hydrology, sustainability. Water Resour. J. Nature Geosci. 10, 71.

Hao, Y., Yeh, T.-C.J., Gao, Z., Wang, Y., Zhao, Y., 2006. A gray system model for studying the response to climatic change: the Liulin karst springs China. J. Hydrol. 328, 668–676. https://doi.org/10.1016/j.jhydrol.2006.01.022.

Hartmann, A., Lange, J., Vivó, À., Mizyed, N., Smiatek, G., Vivó Aguado, À., Mizyed, N., Smiatek, G., Kunstmann, H., 2012. A multi-model approach for improved simulations of future water availability at a large Eastern Mediterranean karst spring. J. Hydrol. 468–469, 130–138. https://doi.org/10.1016/j.jhydrol.2012.08.024.

Hartmann, A., Mudarra, M., Andreo, B., Marín, A., Wagener, T., Lange, J., 2014. Modeling spatiotemporal impacts of hydroclimatic extremes on groundwater recharge at a Mediterranean karst aquifer. Water Resour. Res. 50 (8), 6507–6521.

Hartmann, A., Kobler, J., Kralik, M., Dirnböck, T., Humer, F., Weiler, M., 2016. Model-aided quantification of dissolved carbon and nitrogen release after windthrow disturbance in an Austrian karst system. Biogeosciences 13, 159–174.

Hartmann, A., Barberá, J.-A., Andreo, B., 2017. On the value of water quality data and informative flow states in karst modelling. Hydrol. Earth Syst. Sci. 21, 5971–5985.

Hawkins, E., Osborne, T.M., Ho, C.K., Challinor, A.J., 2013. Calibration and bias correction of climate projections for crop modelling: An idealised case study over Europe. Agr. Forest Meteorol. 170, 19–31.
Iglesias, A., Garrote, L., Flores, F., Moneo, M., 2007. Challenges to manage the risk of water scarcity and climate change in the mediterranean. Water Resour. Manage. 21, 775.
Isotta, F.A., Frei, C., Weilguni, V., Perčec Tadić, M., Lassègues, P., Rudolf, B., Pavan, V., Cacciamani, C., Antolini, G., Ratto, S.M., Munari, M., Micheletti, S., Bonati, V., Lussana, C., Ronchi, C., Panettieri, E., Marigo, G., Vertačnik, G., 2014. The climate of daily precipitation in the Alps: development and analysis of a high-resolution grid dataset from pan-Alpine rain-gauge data. Int. J. Climatol. 34, 1657–1675.
Lauffenburger, Z.H., Gurdak, J.J., Hobza, C., Woodward, D., Wolf, C., 2018. Irrigated agriculture and future climate change effects on groundwater recharge, northern High Plains aquifer, USA. Agric. Water Manage. 204, 69–80.
Khadka, D., Babel, M.S., Shrestha, S., Tripathi, N.K., 2014. Climate change impact on glacier and snow melt and runoff in Tamakoshi basin in the Hindu Kush Himalayan (HKH) region. J. Hydrol. 511, 49–60.
Kiraly, L., 2002. Karstification and Groundwater flow. In: Proceedings of the conference on Evolution of Karst: From Prekarst to Cessation Postojna-Ljubljana, pp. 155–190.
Kløve, B., Pertti Ala-Aho, P., Bertrand, G., Gurdak, J.J., Kupfersberger, H., Kværner, J., Muotka, T., Mykrä, H., Preda, E., Rossi, P., Bertacchi Uvo, C., Velasco, E., Pulido-Velazquez, M., 2014. Climate change impacts on groundwater and dependent ecosystems. J. Hydrol.Part B 518, 250–266.
Kopsiaftis, G., Tigkas, D., Christelis, V., Vangelis, H., 2017. Assessment of drought impacts on semi-arid coastal aquifers of the Mediterranean. J. Arid Environ. 137, 7–15.
Loaiciga, H.A., Maidment, D.R., Valdes, J.B., 2000. Climate-change impacts in a regional karst aquifer, Texas, USA. J. Hydrol. 227, 173–194. https://doi.org/10.1016/S0022-1694(99)00179-1.
Maillet, E., 1905. Essais d'hydraulique souterraine et fluviale. Librairie Sci., A. Hermann, Paris.
Manrique-Alba, A., Ruiz-Yanetti, S., Moutahir, H., Novak, K., De Luis, M., Bellot, J., 2017. Soil moisture and its role in growth-climate relationships across an aridity gradient in semiarid Pinus halepensis forests. Sci. Total Environ. 574, 982–990.
Mountain Research Initiative EDW Working Group, 2015. Elevation-dependent warming in mountain regions of the world. Nat. Clim. Change 5, 424–430.
Nikolaidis, N.P., Bouraoui, F., Bidoglio, G., 2013. Hydrologic and geochemical modeling of a karstic Mediterranean watershed. J. Hydrol. 477, 129–138.
Neves, M.C., Costa, L., Monteiro, J.P., 2016. Climatic and geologic controls on the piezometry of the querença-silves karst aquifer, algarve (Portugal). Hydrogeol. J. 24 (4), 1015–1028.
Ranjan, P.S., Kazama, S., Sawamoto, M., 2006. Effects of climate and land use changes on groundwater resources in coastal aquifers. J. Environ. Manage. 80 (1), 25–35.
Ravbar, N., Kovačič, G., Petrič, M., Kogovšek, J., Brun, C., Koželj, A., 2017. Climatological Trends and Anticipated Karst Spring Quantity and Quality: Case Study of the Slovene Istria. Geological Society London, Special Publications, pp. 466.
Ruane, A.C., Goldberg, R., Chryssanthacopoulos, J., 2015. Climate forcing datasets for agricultural modeling: merged products for gap-filling and historical climate series estimation. Agric. For. Meteorol. 200, 233–248.
Samuels, R., Rimmer, A., Hartmann, A., Krichak, S., Alpert, P., 2010. Climate change impacts on Jordan River flow: downscaling application from a regional climate model. J. Hydrometeorol. 11, 860–879. https://doi.org/10.1175/2010JHM1177.1.
Sapriza-Azuri, G., Jódar, J., Carrera, J., Gupta, H.V., 2015. Toward a comprehensive assessment of the combined impacts of climate change and groundwater pumping on catchment dynamics. J. Hydrol. 529, 1701–1712.
Sharma, B., Jangle, N., Bhatt, N., Dror, D.M., 2015. Can climate change cause groundwater scarcity? An estimate for Bihar. Int. J. Climatol. 35 (14), 4066–4078.
Shrestha, S., Bach, T.V., Pandey, V.P., 2016. Climate change impacts on groundwater resources in Mekong Delta under representative concentration pathways (RCPs) scenarios. Environ. Sci. Policy 61, 1–13.
Stigter, T.Y., Nunes, J.P., Pisani, B., 2014. Comparative assessment of climate change and its impacts on three coastal aquifers in the Mediterranean. Reg. Environ. Change 14 (Suppl 1), 41.
Taylor, et al., 2013. Ground water and climate change. Nat. Clim. Change 3, 322–329.
Van Vuuren, D., Edmonds, J., Kainuma, M., Riahi, K., Thomson, A., Hibbard, K., 2011. The representative concentration pathways: an overview. Clim. Change 109, 5–31.
Xanke, J., Jourde, H., Liesch, T., Goldscheider, N., 2016. Numerical long-term assessment of managed aquifer recharge from a reservoir into a karst aquifer in Jordan. J. Hydrol. 540, 603–614 ISSN 0022-1694.
Yang, T., Wang, X., Yu, Z., Krysanova, V., Chen, X., Schwartz, F.W., Sudicky, E.A., 2014. Climate change and probabilistic scenario of streamflow extremes in an alpine region. J. Geophys. Res. Atmos. 119, 8535–8551.
Zuzel, J.F., Cox, L.M., 1975. Relative importance of meteorological variables in snowmelt. Water Resour. Res. 11 (1), 174–176.